Urban measurements of atmospheric nitrous acid: A caveat on the interpretation of the HONO photostationary state

B. H. Lee,[1] E. C. Wood,[2,3] S. C. Herndon,[3] B. L. Lefer,[4] W. T. Luke,[5] W. H. Brune,[6] D. D. Nelson,[3] M. S. Zahniser,[3] and J. W. Munger[1]

Received 8 June 2013; revised 10 September 2013; accepted 21 October 2013.

[1] Numerous studies infer the existence of an "unknown" daytime HONO source based on the assumption that HONO is at photostationary state (PSS). Secondary HONO production rate as high as 1.1 ppb hr^{-1} can be estimated from this approach, based on measurements made during the Study of Houston Atmospheric Radical Precursors campaign in May of 2009. We argue, however, that the PSS assumption might not have been valid because the transport time from nearby NO_x emission sources to the measurement site was likely less than the time required for HONO in vehicle exhaust to reach PSS. Using a chemical box model, we demonstrate that there is initially net HONO formation as high levels of NO in exhaust react with ambient OH. Net production is followed by a period of net HONO loss dominated by photolysis that is sustained for several minutes to hours depending on time of day. The presence of relatively fresh exhaust in sampled air can partially, if not fully, account for the observed measurement PSS discrepancy. We also show that a large fraction of the observed nighttime increase in $HONO/NO_x$ ratio is explained by NO_2 oxidation. These results do not rule out the existence of an unexplained secondary HONO source but suggest that great care must be exercised when applying the PSS method to quantify its strength.

Citation: Lee, B. H., E. C. Wood, S. C. Herndon, B. L. Lefer, W. T. Luke, W. H. Brune, D. D. Nelson, M. S. Zahniser, and J. W. Munger (2013), Urban measurements of atmospheric nitrous acid: A caveat on the interpretation of the HONO photostationary state, *J. Geophys. Res. Atmos.*, *118*, doi:10.1002/2013JD020341.

1. Introduction

[2] Measurements of urban HONO concentrations by a variety of detection techniques indicate it to be a significant daytime source of hydroxyl radicals (OH) in the troposphere [*Mao et al.*, 2010; *Ren et al.*, 2003, 2006]. The three gas-phase reactions that are typically considered to govern daytime HONO levels are formation by the reaction between nitric oxide (NO) and OH (R1) and losses by photolysis (R2) and oxidation (R3) by OH.

(R1) $OH + NO + M \rightarrow HONO + M$ $\quad k_1$

(R2) $HONO + h\nu \rightarrow OH + NO$ $\quad J_{HONO}$

(R3) $HONO + OH \rightarrow H_2O + NO_2$ $\quad k_3$

[3] At photostationary state (PSS), the instantaneous net time rate of concentration change due to chemistry, illustrated by equation (1), is zero. Observations of negative instantaneous net rates (equation (1) < 0)—which are constrained by measurements of [OH], [NO], [HONO], and J_{HONO}—have been interpreted as evidence of an unaccounted HONO source so as to maintain PSS [*Alicke et al.*, 2002; *Sorgel et al.*, 2011; *Wong et al.*, 2012]. Numerous formation pathways have been proposed to reconcile the observed imbalance between production (R1) and destruction (R2 + R3), including heterogeneous reaction enhanced by photoexcited organics [*Stemmler et al.*, 2006, 2007], the reaction of electronically excited nitrogen dioxide (NO_2) with water vapor [*Li et al.*, 2008], soil emissions [*Su et al.*, 2011], production on soot surfaces [*Monge et al.*, 2010], and heterogeneous nitrate ion photolysis [*Zhou et al.*, 2011; *Ziemba et al.*, 2010].

$$\frac{d[HONO]}{dt} = k_1[OH][NO] - J_{HONO}[HONO] - k_3[OH][HONO] \quad (1)$$

[4] Moreover, nighttime accumulation of HONO—which initiates photochemistry in the early morning prior to other

[1]School of Engineering and Applied Science, Harvard University, Cambridge, Massachusetts, USA.
[2]Department of Public Health, University of Massachusetts, Amherst, Massachusetts, USA.
[3]Center for Atmospheric and Environmental Chemistry, Aerodyne Research, Inc., Billerica, Massachusetts, USA.
[4]Department of Earth and Atmospheric Sciences, University of Houston, Houston, Texas, USA.
[5]Air Resources Laboratory, National Oceanic and Atmospheric Administration, Silver Spring, Maryland, USA.
[6]Department of Meteorology, Pennsylvania State University, University Park, PA, USA.

Corresponding author: B. H. Lee, School of Engineering and Applied Science, Harvard University, 20 Oxford Street, Cambridge, MA 02138, USA. (benhlee@u.washington.edu)

©2013. American Geophysical Union. All Rights Reserved.
2169-897X/13/10.1002/2013JD020341

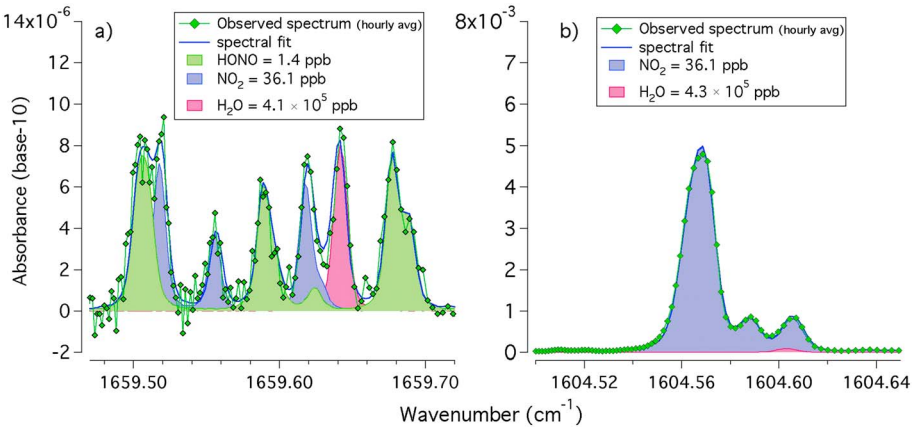

Figure 1. One hour averaged absorbance (=$\log_{10}(\sigma nl)$, where σ=absorption cross section, n = number density, and l = pathlength) spectra of (a) HONO and (b) NO_2. The color-filled areas are simulated absorbances based on known line positions and strengths obtained by nonlinear fits to the observed spectra (green markers). The water vapor absorbances are not absolute values but represent the water vapor content difference between ambient and zero air. The relatively weak NO_2 absorption lines near those of HONO in the 1659.50 to 1659.70 cm^{-1} spectral range are fit in real time with number density values obtained by the strong NO_2 absorption lines near 1604.55 cm^{-1} to ensure minimal interference on HONO. These two spectra represent the time period between 1:30 and 2:30 A.M. CST on 28 May 2009.

HO_x precursors [*Winer and Biermann*, 1994]—has been largely attributed to NO_2-driven heterogeneous hydrolysis with negligible contribution from combustion sources [*Platt et al.*, 1980; *Yu et al.*, 2009]. This assertion is based on ambient observations of HONO to NO_x ratios—in excess of those reported in fresh vehicle exhaust—that increase following sunset.

[5] We present midinfrared absorption spectroscopic measurements of NO_2 and HONO mixing ratios during the Study of Houston Atmospheric Radical Precursors (SHARP) campaign during May of 2009 and interpret them in simple modeling analyses that challenge the assumptions on which assessment of secondary day and nighttime HONO production are based.

2. Experiment

2.1. Field Measurements

[6] Measurements were made atop the North Moody Tower (70 m a.g.l.) on the University of Houston campus, situated approximately 5 km southeast of downtown (latitude 29.72°; long. −95.34°). Mixing ratios of HONO and NO_2 were simultaneously quantified using a dual tunable infrared quantum cascade laser absorption spectrometer, capable of fast time-response measurements without derivatization or extraction into the liquid phase. Figure 1 shows typical 1 h averaged spectra of HONO and NO_2 recorded during SHARP. Ambient air was drawn from the top of a four-story scaffolding tower through a custom-built quartz inlet, connected by 30 ft (9.2 m) of 3/8 in. (9.5 mm) outer diameter perfluoroalkoxy tubing to the spectrometer, which was housed in an air-conditioned shed on the roof of the 18-story building. The inlet removed particles larger than about 4 microns from the sample stream by inertial separation, obviating the need for filters. A critical orifice at the inlet reduced the pressure to about 0.5 bar. Both the inlet and tubing were heated to 35°C and covered by opaque materials. The combination of reduced pressure and heating minimized the presence of aqueous films in the sample line.

[7] Though the spectroscopic technique minimizes interferences, the potential remains for sampling artifacts. These were assessed by routine in situ tests that challenged the sample line. Routine additions of humidity-matched zero air and gaseous HONO and NO_2 consistently showed equal response times for HONO and NO_2 through the inlet, tubing, and sample cell, indicating no reversible loss of HONO during sampling [*Lee et al.*, 2011, Figure 5]. Introducing NO_2 levels >200 ppb mixed with ambient Houston air under conditions conducive to heterogeneous chemistry (i.e., unheated tubing, sample near ambient pressure) showed no evidence of HONO production [*Lee et al.*, 2011, Figure 6]. Additions from a stable source of HONO in laboratory studies exhibited no instantaneous loss due to either the inlet or the tubing. The sample residence (1/e) times in the inlet, tubing, and cell were on average 0.3, 0.2, and 1.3 s, respectively, at a total flow rate of approximately 10 standard liters per minute. The instrumental detection limits (3σ) with 1 h spectral averaging were 40 ppt and 10 ppt (pmol/mol) for HONO and NO_2, respectively, during SHARP. The overall uncertainties in the hourly averaged HONO and NO_2 measurement are estimated at 12% and 8%, respectively.

[8] Quantification of HONO in the field relied on the accuracy of midinfrared line strengths obtained in the laboratory by measuring the absorbance of HONO by the spectrometer while quantifying HONO by complete catalytic conversion to NO, followed by calibrated absorption spectroscopy [*Lee et al.*, 2012]. Comparison to four unique point measurement instruments included in the SHARP campaign corroborates the instrument accuracy. A long path-averaged differential optical absorption spectroscopy measurement was typically lower than the point measurement methods, due likely to heterogeneity along its absorption path that is not represented by the point measurements. Detailed

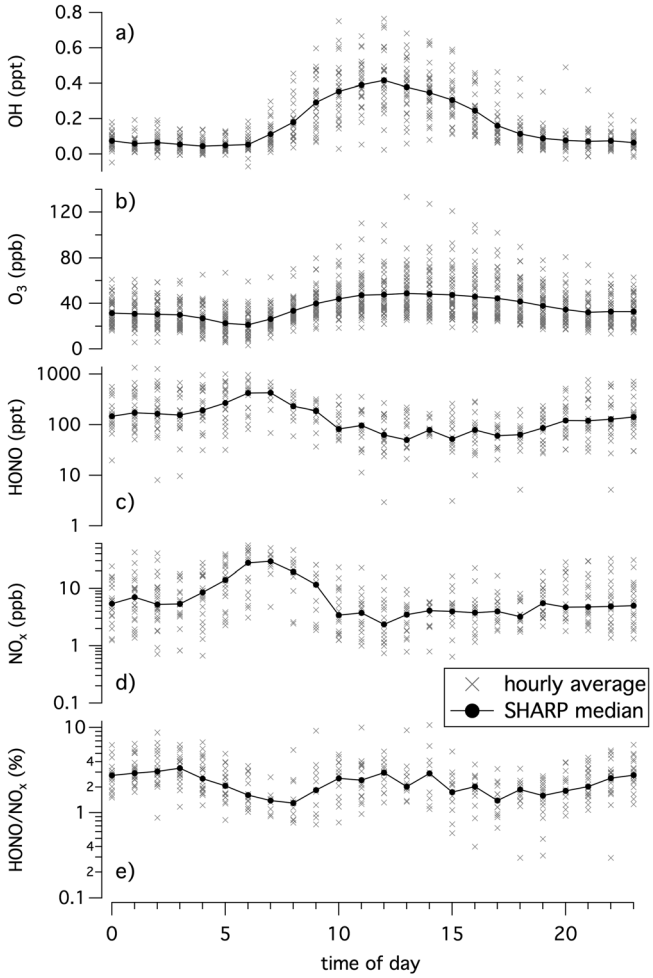

Figure 2. Observed mixing ratios of (a) OH, (b) O_3, (c) HONO, (d) NO_x, and (e) ratio of HONO/NO_x. Individual points (grey cross) represent hourly averages, while the solid line (black dot) shows the overall median for the entire campaign.

analyses on the intercomparison are presented by Pinto et al. (unpublished data, 2013).

[9] Other variables utilized in the present analysis include measurements of OH by laser-induced fluorescence [*Mao et al.*, 2010], NO by ozone chemiluminescence [*Luke et al.*, 2010] and HONO photolysis rates, derived from measured NO_2 photolysis rates using the parameterization of *Kraus and Hofzumahaus* [1998]. All three in situ measurements were obtained by instruments colocated with the HONO inlet on the scaffolding tower.

2.2. Model Description

[10] A box model was used to determine the time evolution of HONO, NO, and NO_2, mixing ratios in vehicle exhaust, the dominant source of nitrogen oxides in the region, mixing into HONO and NO_x-free background air. Only reactions R1 to R6 were considered, with rates for 298 K [*Atkinson et al.*, 2004; *Sander et al.*, 2011].

(R4) $NO + O_3 \rightarrow NO_2 + O_2$ k_4
(R5) $NO_2 + hn \rightarrow NO + O$ k_5
(R6) $NO_2 + OH + M \rightarrow HNO_3 + M$ k_6

[11] Dilution at each time step was simulated for the simplest case of a ground-level emission source with no effective plume rise using the dispersion equation

$$\text{dilution factor} = \frac{\sigma_z(t)\sigma_y(t)}{\sigma_z(t-1)\sigma_y(t-1)} \quad (2)$$

$$\sigma_y(x) = ax^{0.894} \quad (3)$$

$$\sigma_z(x) = cx^{\mathrm{d}} + f \quad (4)$$

summarized in *Turner* [1994], where x is distance in km and σ_y and σ_z are the horizontal crosswind and vertical dispersion coefficients. Distance was transformed to time assuming a constant wind speed of 5.5 m s^{-1}, the median midday wind speed observed during SHARP. Constants a (213), c (440.8 at $x < 1$ km; 459.7 at $x > 1$ km), d (1.941 at $x < 1$ km; 2.094 at $x > 1$ km), and f (9.27 at $x < 1$ km; −9.6 at $x > 1$ km) for the "very unstable" atmospheric stability case were used as the base case. The same dilution rate was used to simulate the entrainment of 0.4 ppt and 40 ppb of background OH and O_3—median daytime levels observed during SHARP (Figures 2a and 2b)—into the exhaust plume that is initially free of OH and O_3. The initial NO/NO_2/HONO distribution (0.95/0.042/0.008) in exhaust was obtained from *Kurtenbach et al.* [2001]. The initial emitted sum of model NO, NO_2, and HONO was 100 ppm. The HONO photolysis rate was kept constant at a typical noontime value of 1.6×10^{-3} s^{-1}. Sensitivity test results of the rate of mixing, OH, J_{HONO} and initial emitted NO_x on the extent of deviation from PSS and the rate at which PSS is approached are discussed in the following section.

[12] For the nighttime box model simulations, the initial [NO], [NO_2], and HONO/NO_x ratio at sunset (19:00) for all cases was set to their corresponding observed median values (0.3 ppb, 4.6 ppb, 1.6%). The mixing ratios of NO, NO_2, NO_3, and N_2O_5 were calculated over an 8 h period at 1 s time steps, taking into account reactions R7 to R11. Levels of O_3 were held constant at 30 ppb throughout the simulation, as no significant nighttime trend was observed during SHARP (Figure 2b). Dilution was excluded to simulate chemistry occurring in a stagnant nighttime air mass. Three sets of model runs were conducted with (1) chemistry only, (2) chemistry and deposition of HONO and NO_x, and (3) chemistry, deposition, and emission from automobiles.

(R7) $NO + O_3 \rightarrow NO_2 + O_2$ k_7
(R8) $NO_2 + O_3 \rightarrow NO_3 + O_2$ k_8
(R9) $NO + NO_3 \rightarrow NO_2 + NO_2$ k_9
(R10) $NO_2 + NO_3 + M \rightarrow N_2O_5 + M$ k_{10}
(R11) $N_2O_5 + M \rightarrow NO_2 + NO_3 + M$ k_{11}

3. Results

3.1. Daytime

[13] Figure 3a shows d[HONO]/dt (equation (1)) calculated using observed hourly averages of [NO], [OH], [HONO], and J_{HONO}. This instantaneous net rate, as it is referred to henceforth, was typically negative during SHARP. Barring an overestimation of the HONO loss rate, an unknown secondary HONO source as high as 1.1 ppb hr^{-1} would be required if the system was actually in a photostationary state (PSS). However, to be in PSS, the time of the observation—

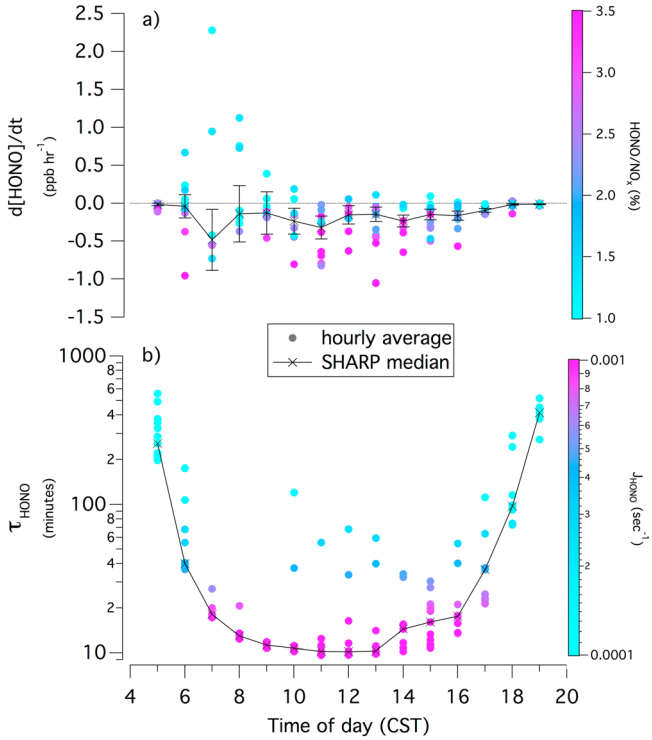

Figure 3. (a) Calculated d[HONO]/dt values (equation (1)) based on observed hourly averages of [OH], [NO], [HONO], and J_{HONO}, colored by measured HONO/NO_x values. If PSS is assumed, periods when d[HONO]/dt is negative indicate an unaccounted HONO source. (b) Calculated atmospheric lifetime of HONO (equation (5)), colored by measured J_{HONO} values. Both Figures 3a and 3b are plotted as a function of time of day. Individual points (grey cross) represent all of the hourly averages calculated during periods of NO, OH, HONO, and J_{HONO} data overlap. The solid line (black dot) shows the overall median for the entire SHARP campaign. The error bars in Figure 3a are the mean uncertainty of the hourly d[HONO]/dt values, considering the errors associated with NO (7%), OH (15%), and HONO (12%) [*Luke et al.*, 2010; *Kovacs et al.*, 2003].

or reaction time since emission/production—must be several times longer than the lifetime of the species being considered [*Steinfeld et al.*, 1989; *Turanyi et al.*, 1993]. The HONO lifetime, τ_{HONO}, defined as the inverse sum of its loss rates (equation (5)), ranged from about 10 min at midday to several hours during the early morning and late afternoon periods (Figure 3b).

$$\tau_{HONO} = \frac{1}{\sum_i k_i} = \frac{1}{J_{HONO} + k_3[OH]} \quad (5)$$

[14] Figure 4a (black) shows the time evolution of the modeled instantaneous net rate—d[HONO]/dt—of vehicle exhaust initially containing 100 ppm of the sum of NO, NO_2, and HONO and devoid of OH and O_3, diluting into a very unstable atmosphere with a background of 0.4 ppt and 40 ppb of OH and O_3, respectively. There is initially net HONO production (equation (1) > 0) immediately following emission as the rate of reaction R1 exceeds the sum of the rates of R2 and R3. As NO is depleted by dilution and reaction with O_3 (R4) and OH (R1), this short time period (on the order of a few minutes) of net HONO production is followed by a longer period (on the order of several minutes) when d[HONO]/dt is negative (equation (1) < 0) due to R2 and R3. Under these conditions, a minimum d[HONO]/dt value of −0.30 ppb hr^{-1} is obtained 2.5 min (= t_{min}) following emission and exponentially decreases to 1/e of the minimum value after another 1.5 min (= τ_e) en route to establishing PSS (equation (1) ~ 0). The main implication of this exercise is that there exists a window of time in which d[HONO]/dt is negative. Erroneously assuming the presence of PSS during this time period would lead to overestimates of secondary HONO sources.

[15] Under the base case conditions considered above, the level of modeled NO_x decreases to below ppb levels within 10 min following emission (Figure 5). The typical midday NO_x mixing ratio observed during SHARP was around 5 ppb (Figure 2d), which according to the modeled time series (Figure 5) would infer a photochemical lifetime since emission of about 5 min. At this time, the modeled d[HONO]/dt is −0.06 ppb hr^{-1} (Figure 4a), comparable to the observed median midday d[HONO]/dt value of −0.1 ppb hr^{-1} (Figure 3a). The estimated photochemical lifetime would be even shorter, hence, the modeled d[HONO]/dt is more negative if the reactions involving NO_x forming reservoir or sink species such as organic nitrates were to be included in the model. The presence of significant levels of NO_x in nonexhaust background air would increase the NO_x concentration and—ignoring the effects of entrained NO on HONO production and lifetime—would imply a longer photochemical lifetime. However, the typical midday HONO/NO_x ratio observed during SHARP (Figure 2e) was 2–3%, while the modeled ratio at its peak, which occurs at about the same time as the minimum d[HONO]/dt, is only about 1% (Figure 4b). Given that the HONO/NO_x ratio in unperturbed background air is likely lower than what is found in vehicle exhaust (0.8%) [*Kurtenbach et al.*, 2001] due to lower levels of hypothesized HONO precursors (e.g., NO_x and soot particles) and the proximity of direct emission sources to the measurement site, we posit negligible contribution of HONO and NO_x from the entrainment of background air. Last, if the model was initiated with a sum of NO, NO_2, and HONO greater than 100 ppm, the ppb threshold would be reached later in simulation time, also indicating an older photochemical lifetime. However, the absolute value of d[HONO]/dt would also increase—linearly in the current model since OH and O_3 levels are prescribed—resulting in a more negative d[HONO]/dt value.

[16] The base case scenario described above likely represents a lower limit in the extent and duration of deviation from PSS. First, the dilution rate in the very unstable atmosphere of *Turner* [1994] likely represents an upper limit to mixing in this setting. For instance, the University of Houston campus is approximately 5 km southeast of the center of Houston and is within 5 km of major freeways in all directions. Assuming that emission sources located within this perimeter are responsible for the observed enhancements of HONO and NO_x mixing ratios and given a constant SHARP-averaged daytime wind speed of 5.5 m s^{-1}, the mean transport time for the emitted species is approximately 15 min, which is comparable but slightly longer than the 5

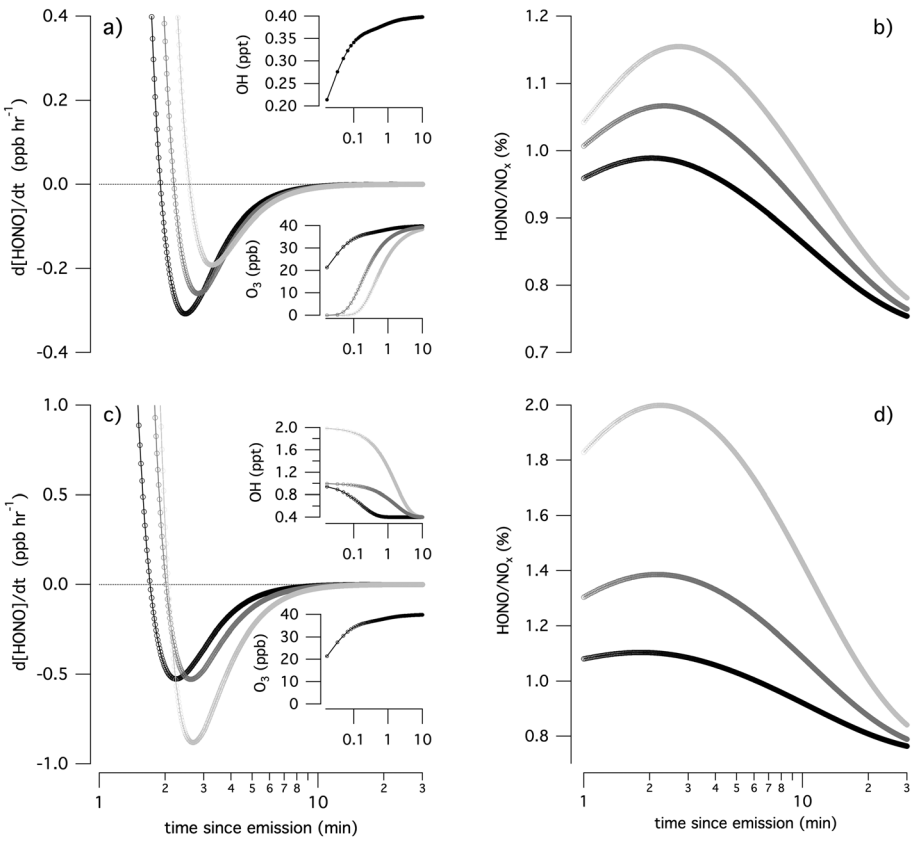

Figure 4. (a and c) Time series of box model d[HONO]/dt and (b and d) HONO/NO_x ratio. The black traces in Figures 4a and 4b represent the results from the base case. The lower inset in Figure 4 shows the O_3 values used to obtain the corresponding results shown in Figures 4a and 4b. The upper inset in Figure 4c shows the OH values used to obtain the corresponding results shown in Figures 4c and 4d. For all conditions, d[HONO]/dt is negative for a period of time, during which sampling vehicle exhaust can lead to overestimates of secondary HONO sources if a photostationary state is inappropriately assumed.

min photochemical lifetime derived from the very unstable atmosphere approximation above. A slower dilution rate would be consistent with a longer photochemical lifetime. Figure 6 (red) shows the minimum d[HONO]/dt value and the sum of the time at which the minimum d[HONO]/dt is obtained (t_{min}) and the subsequent time (τ_e) needed to reach 1/e of this minimum, as a function of mixing rate relative to the base case. As dilution is slowed, the minimum d[HONO]/dt value becomes increasingly negative, since more NO is present—particularly during the initial stages following emission—to react with OH to form HONO. PSS is also approached more slowly with slower mixing, since it takes longer for OH and O_3, the primary oxidants of NO, to reach their respective steady state background values.

[17] Second, the modeled levels of OH and O_3 are unaffected by the initial sum of emitted NO_x, since we essentially simulate a single parcel of exhaust diluting into an infinite background reservoir of OH and O_3. In actuality, O_3 levels are likely suppressed within congested emission source regions by high levels of NO. Additionally, the model assumes complete mixing at every time step, though the rate of the chemical reaction between NO and O_3 is likely much faster than the rate of mixing. This in effect segregates NO and O_3 resulting in a slower reaction [*Damköhler*, 1940], allowing more of the NO to react with OH to form HONO. Figure 4a shows the time evolution of d[HONO]/dt as O_3 is allowed to reach its steady state value at three different rates. The slower the approach of O_3 to its background level, the longer it takes d[HONO]/dt to establish PSS. The absolute value of d[HONO]/dt is less negative than the base case since less O_3 allows more NO to be present without immediately affecting the other species.

[18] Last, OH levels immediately following emission are likely to be higher due to photolysis of concentrated levels of HONO from emission and formation by R1, as well as due to directly emitted OH [*Smith and Starkman*, 1969]. Figure 4c illustrates that with greater enhancement of OH following emission and the longer that it is sustained, d[HONO]/dt will be more negative and take longer to reach PSS due to greater production of HONO by the homogeneous reaction between NO and OH (R1).

[19] Figures 2e and 3a show the diurnal trends of HONO/NO_x ratio and d[HONO]/dt, respectively, both with enhanced values during daytime over the early morning/late afternoon periods. Previous studies have attributed such observations to the existence of a sunlight-driven secondary HONO source with NO_2 as the precursor [*Wong et al.*, 2012]. Our simulations, however, show that the oxidation of NO by OH to form HONO in the early stages following emission results in an increase in the HONO/NO_x ratio to levels above what has been reported in automobile exhaust. With increased OH and/or the suppression of O_3 levels during this initial mixing

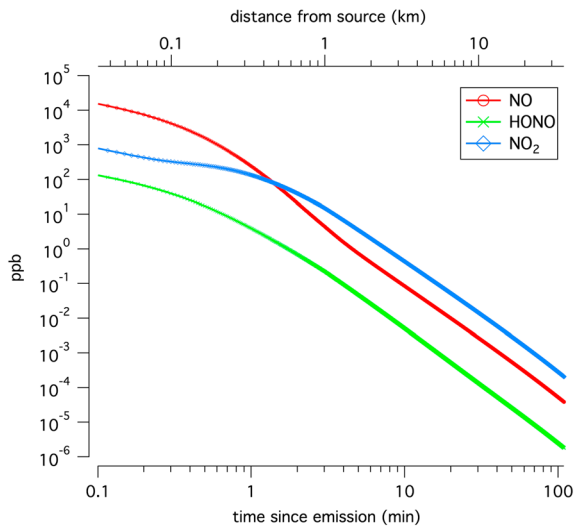

Figure 5. Box model time series of NO, NO_2, and HONO mixing ratios under the base case (100 ppm of sum of NO, NO_2, and HONO emitted; zero OH and O_3 in the initial exhaust; background OH and O_3 of 0.4 ppt and 40 ppb, respectively; only reactions R1-R6 considered; dilution rate simulated under the very unstable atmosphere summarized in *Turner* [1994]). Distance from emission source (top axis) was calculated from time since emission, assuming a constant wind speed of 5.5 m s^{-1}.

period, the HONO/NO_x ratio can increase to values observed during SHARP (Figures 4b and 4d) even without the inclusion of NO_x loss pathways such as the formation of organic nitrates. Conversely, lower OH and J_{HONO} levels result in the decrease of both d[HONO]/dt and HONO/NO_x ratio and the lengthening of the time required to establish PSS, as the three terms on the right-hand side of equation (1) approach zero, illustrated in Figure 6 (black). Hence, the observed diurnal trends of HONO/NO_x and d[HONO]/dt can be explained without invoking an unknown secondary source of HONO. Last, under low J_{HONO} and high NO conditions, a positive d[HONO]/dt can be sustained as R1 always exceeds the sum of R2 and R3 (not pictured). This can explain the few instances of positive d[HONO]/dt events during the early morning rush hour periods (Figure 3a).

[20] Both the extent and duration of deviation from PSS are sensitive to the age of the sampled air mass and the photochemical conditions within the plume. Accurately capturing the history of chemistry and mixing, the complex distribution of photochemical ages and the variability in source strengths and their chemical signatures is outside the scope of a simple chemical box model. This makes it difficult to directly compare model-derived values of d[HONO]/dt (Figures 4a and 4c) to those calculated with observed concentrations (Figure 3a). These simulations nonetheless illustrate that (1) PSS is not achieved instantaneously following emission and that (2) under reasonable conditions of the mixing rate and the levels of OH and O_3 in fresh exhaust, the PSS assumption may not be valid when sampling within an urban setting.

3.2. Nighttime

[21] The HONO/NO_x ratio on average increased between sunset and about 3 A.M. during SHARP (Figure 7a). Previous studies have attributed similar observations to heterogeneous HONO production by NO_2 on the ground [*Wong et al.*, 2011] or aerosol [*Yu et al.*, 2009] surfaces. Direct emissions were discounted when estimating production rates because observed HONO/NO_x ratios exceeded those reported in vehicle exhaust. The average nighttime conversion rate of NO_2 to HONO has been previously estimated by calculating the increase in HONO concentration over some time period following sunset normalized by a nighttime average NO_2 value (ppb HONO produced per ppb NO_2 present per hour) [*Alicke et al.*, 2002, equation (17)]. However, neither the chemical processing of directly emitted NO_x nor its deposition, the presumed source of HONO production, was taken into account. We consider nocturnal chemistry of NO_x associated with NO_3 and N_2O_5 formation (R7-R11) in a box model to estimate HONO production per NO_2 deposited in a well-mixed stagnant nighttime air mass.

[22] Figure 7a shows results from three simulations of HONO/NO_x ratios following nightfall. The base case (red) considers only O_3-initiated NO_x oxidation (R7-R11) and exhibits an increasing trend in HONO/NO_x that is comparable

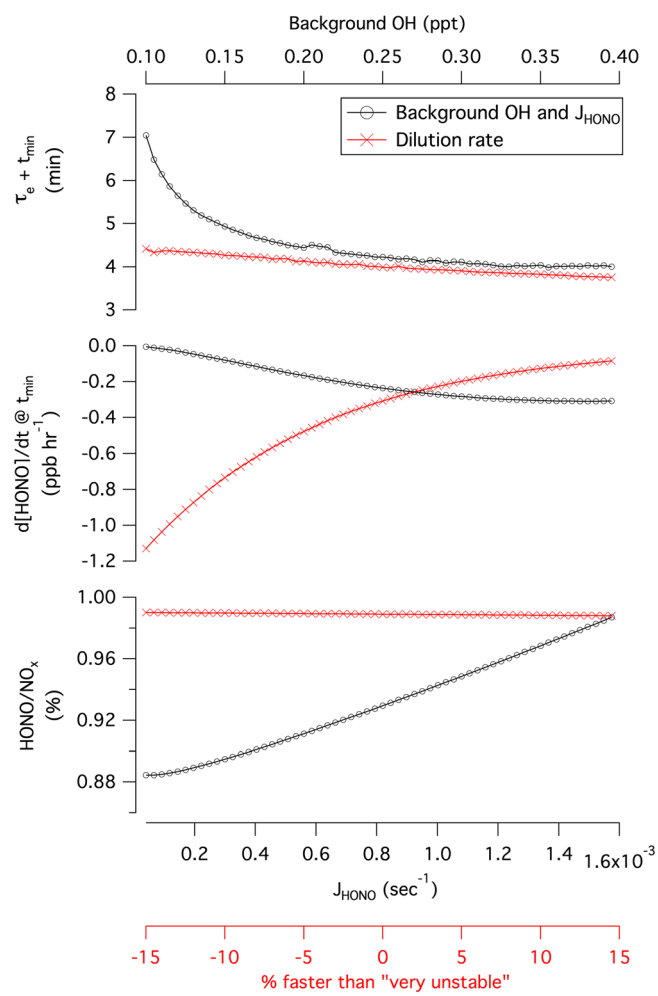

Figure 6. Sensitivity of the sum of τ_e and t_{min}, d[HONO]/dt at t_{min}, and maximum HONO/NO_x ratio. The black traces show the simultaneous sensitivity to OH (top axis) and J_{HONO} (bottom black axis), which are covarying. The red trace is plotted against rate of mixing relative to the very unstable base case (red axis).

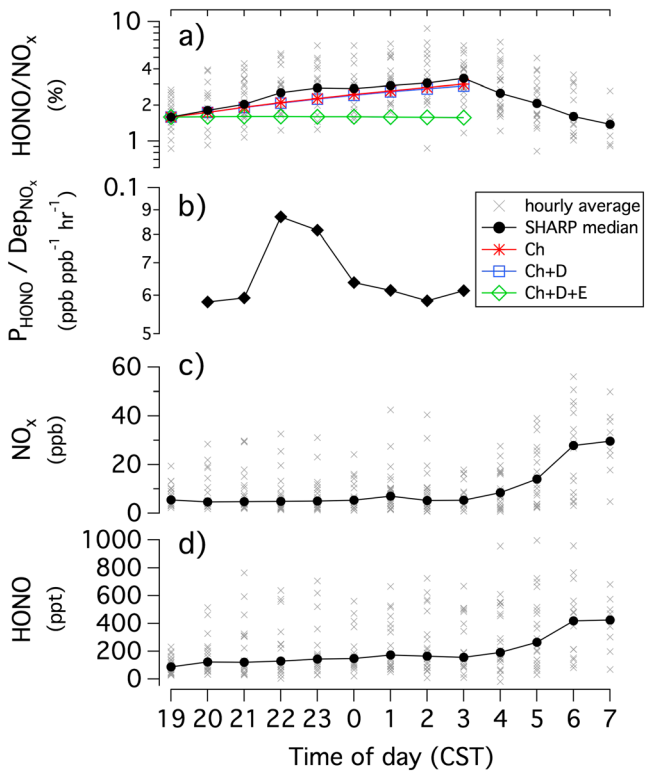

Figure 7. (a) The observed (black circles) and modeled (chemistry only (red); chemistry + deposition (blue); chemistry + deposition + emissions (green)) HONO/NO_x ratio, (b) calculated HONO produced per NO_2 deposited per hour, (c) observed NO_x, and (d) HONO mixing ratios. Individual points (grey cross) represent hourly averages during periods of NO, NO_2, and HONO data overlap. The solid line (black dot) shows the overall median for the entire SHARP campaign. Near 03:00 CST, HONO and NO_x mixing ratios increase while the HONO/NO_x ratio decreases, indicating increasing influence of freshly emitted NO_x.

to observed patterns. Including deposition of HONO and NO_2, both with a deposition velocity of 0.1 cm s^{-1} [*Stutz et al.*, 2002] integrated over a 100 m boundary layer height, does not significantly alter the HONO/NO_x trend (blue). In both cases, however, the resulting NO_x level decays to about half the initial value mainly due to conversion of NO_x to NO_3 and N_2O_5. Observed NO_x levels, however, do not show consistent nighttime decreases (Figure 7c). Maintaining a constant simulated NO_x level by replacing the NO_x lost to chemical reaction and deposition with fresh emissions that have a HONO/NO_x ratio of 0.008 [*Kurtenbach et al.*, 2001] results in a lower simulated HONO/NO_x trend (green). We interpret the difference between the median of the SHARP observations (black) and this modeled scenario that includes chemistry, deposition, and emissions (green) as secondary nighttime HONO production. The change in NO_x mixing ratio due to chemistry, deposition, and emission over the 8 h period from 19:00 to 03:00 is −2.4 ppb, −0.6 ppb, and +3.0 ppb, respectively, while the change in HONO concentration due to deposition, emission, and secondary production is −20 ppt, +40 ppt, and +90 ppt, respectively.

[23] Figure 7b shows the rate of increase in HONO/NO_x not attributable to NO_2 oxidation, deposition, or emission that is the amount of HONO produced by a secondary source per NO_x deposited per hour. This NO_x to HONO conversion rate is on average about 7×10^{-2} ppb HONO per ppb NO_2 per hour, or 1 HONO produced per 15 NO_2 deposited per hour, which is about twice the rate of 1 to 33 reported by *Stutz et al.* [2002]. Given the simplification of the chemistry and assumption of a stagnant air mass, this difference may not be significant. Assuming the lifetimes of NO_3 and N_2O_5 due to reactions and deposition are 2 and 15 min [*McLaren et al.*, 2010], respectively, the estimated rate decreases to 6×10^{-2} ppb HONO produced per NO_2 deposited per hour, since more NO_x is present as the rate of R10 slows, thereby narrowing the difference between the modeled (Figure 7a, green) and observed (Figure 7a, black) HONO/NO_x ratios. Similarly, a decrease in the nighttime O_3 level would slow the rate of NO_x oxidation, requiring less automobile emission, which has a lower HONO/NO_x ratio than the nighttime atmosphere, to maintain a constant level of NO_x (Figure 7c). This results in a simulated HONO/NO_x ratio that is closer to the observed, implying a slower HONO production rate with decreasing ambient O_3. Last, the production rate would be higher if there are unaccounted nighttime HONO loss pathways besides deposition.

4. Conclusion

[24] Using a simple chemical box model based on conservative approximations of chemistry and mixing of automobile exhaust, we have shown that negative instantaneous net rates of HONO concentration change, d[HONO]/dt, are sustained without invoking a secondary HONO source for periods likely longer than the typical photochemical plume age encountered during SHARP. The diurnal trends of HONO/NO_x ratio and d[HONO]/dt can also be explained solely with known chemistry. While these results do not rule out heterogeneous HONO formation, assuming HONO to be completely at PSS will likely overestimate the source strength. If the observed negative instantaneous net rates are entirely the result of sampling exhaust prior to its establishing PSS, then HONO in urban atmospheres is simply a reservoir (a sink near emissions and source downwind) for previously existing HO_x. This analysis points to the importance of explicitly considering the effects of mixing and transport in the near field, particularly when sampling in close proximity to emission sources. During nighttime, we show that NO_x oxidation as well as emissions of HONO and NO_x can significantly affect the HONO/NO_x ratio. Thus, NO_x cannot be considered as a conserved tracer for using the HONO/NO_x ratio as an indicator of HONO production. We estimate that 1 HONO molecule is produced per 15 NO_2 molecules deposited per hour.

[25] **Acknowledgments.** The authors gratefully acknowledge all of the participants of the SHARP campaign. This work was supported by the National Science Foundation (Awards AGS-0813617 and 0814202). Additional funding for the SHARP campaign was provided by the Houston Advanced Research Center grant H113.

References

Alicke, B., U. Platt, and J. Stutz (2002), Impact of nitrous acid photolysis on the total hydroxyl radical budget during the Limitation of Oxidant Production/Pianura Padana Produzione di Ozono study in Milan, *J. Geophys. Res.*, *107*(D22), 8196, doi:10.1029/2000JD000075.

Atkinson, R., D. L. Baulch, R. A. Cox, J. N. Crowley, R. F. Hampson, R. G. Hynes, M. E. Jenkin, M. J. Rossi, and J. Troe (2004), Evaluated kinetic

and photochemical data for atmospheric chemistry: Volume I—Gas phase reactions of O_x, HO_x, NO_x and SO_x species, *Atmos. Chem. Phys.*, *4*, 1461–1738.

Damköhler, G. (1940), Der Einfluss der Turbulenz auf die Flammengeschwindigkeit in Gasgemischen, Zeitschrift für Elektochemie und angewandte Physikalische Chemie, *46*, 601–626.

Kovacs, T. A., et al. (2003), Direct measurements of urban OH reactivity during Nashville SOS in summer 1999, *J. Environ. Monit.*, *5*, 68–74, doi:10.1039/b204339d.

Kraus, A., and A. Hofzumahaus (1998), Field measurements of atmospheric photolysis frequencies for O_3, NO_2, HCHO, CH_3CHO, H_2O_2, and HONO by UV spectroradiometry, *J. Atmos. Chem.*, *31*(1–2), 161–180, doi:10.1023/A:1005888220949.

Kurtenbach, R., K. H. Becker, J. A. G. Gomes, J. Kleffmann, J. C. Lorzer, M. Spittler, P. Wiesen, R. Ackermann, A. Geyer, and U. Platt (2001), Investigations of emissions and heterogeneous formation of HONO in a road traffic tunnel, *Atmos. Environ.*, *35*(20), 3385–3394, doi:10.1016/S1352-2310(01)00138-8.

Lee, B. H., E. C. Wood, M. S. Zahniser, J. B. McManus, D. D. Nelson, S. C. Herndon, G. W. Santoni, S. C. Wofsy, and J. W. Munger (2011), Simultaneous measurements of atmospheric HONO and NO_2 via absorption spectroscopy using tunable mid-infrared continuous-wave quantum cascade lasers, *Appl. Phys. B Lasers Opt.*, *102*(2), 417–423, doi:10.1007/s00340-010-4266-5.

Lee, B. H., E. C. Wood, M. S. Zahniser, J. Wormhoudt, S. C. Wofsy, and J. W. Munger (2012), Effective line strengths of trans-nitrous acid near 1275 cm^{-1} and cis-nitrous acid at 1660 cm^{-1}, *J. Quant. Spectrosc. Radiat. Transfer*, *113*, 1905–1912, doi:10.1016/j.jqsrt.2012.06.004.

Li, S. P., J. Matthews, and A. Sinha (2008), Atmospheric hydroxyl radical production from electronically excited NO_2 and H_2O, *Science*, *319*(5870), 1657–1660, doi:10.1126/science.1151443.

Luke, W. T., P. Kelley, B. L. Lefer, J. Flynn, B. Rappengluck, M. Leuchner, J. E. Dibb, L. D. Ziemba, C. H. Anderson, and M. Buhr (2010), Measurements of primary trace gases and NO_y composition in Houston, Texas, *Atmos. Environ.*, *44*(33), 4068–4080, doi:10.1016/j.atmosenv.2009.08.014.

Mao, J. Q., et al. (2010), Atmospheric oxidation capacity in the summer of Houston 2006: Comparison with summer measurements in other metropolitan studies, *Atmos. Environ.*, *44*(33), 4107–4115, doi:10.1016/j.atmosenv.2009.01.013.

McLaren, R., P. Wojtal, D. Majonis, J. McCourt, J. D. Halla, and J. Brook (2010), NO_3 radical measurements in a polluted environment: Links to ozone formation, *Atmos. Chem. Phys.*, *10*, 4187–4206, doi:10.5194/acp-10-4187-2010.

Monge, M. E., B. D'Anna, and C. George (2010), Nitrogen dioxide removal and nitrous acid formation on titanium oxide surfaces—An air quality remediation process?, *Phys. Chem. Chem. Phys.*, *12*(31), 8992–8999, doi:10.1039/b925785c.

Platt, U., D. Perner, G. W. Harris, A. M. Winer, and J. N. Pitts (1980), Observations of nitrous-acid in an urban atmosphere by differential optical-absorption, *Nature*, *285*(5763), 312–314, doi:10.1038/285312a0.

Ren, X. R., et al. (2003), OH and HO_2 chemistry in the urban atmosphere of New York City, *Atmos. Environ.*, *37*(26), 3639–3651, doi:10.1016/S1352-2310(03)00459.

Ren, X. R., et al. (2006), Behavior of OH and HO_2 in the winter atmosphere in New York City, *Atmos. Environ.*, *40*, S252–S263, doi:10.1016/j.atmosenv.2005.11.073.

Sander, S. P., et al. (2011), Chemical kinetics and photochemical data for use in atmospheric studies, Evaluation No. 17, edited by J. P. Laboratory, JPL Publication 10–6, Pasadena.

Smith, D. S., and E. S. Starkman (1969), Spectroscopic method for simultaneous determination of species concentration and temperature in a cyclic combustion process, *Rev. Sci. Instrum.*, *40*(12), 1541–1544, doi:10.1063/1.1683857.

Sorgel, M., et al. (2011), Quantification of the unknown HONO daytime source and its relation to NO_2, *Atmos. Chem. Phys.*, *11*(20), 10,433–10,447, doi:10.5194/acp-11-10433-2011.

Steinfeld, J. I., J. S. Francisco, and W. L. Hase (1989), *Chemical Kinetics and Dynamics*, vol. xii, pp. 548, Prentice Hall, Englewood Cliffs, N.J.

Stemmler, K., M. Ammann, C. Donders, J. Kleffmann, and C. George (2006), Photosensitized reduction of nitrogen dioxide on humic acid as a source of nitrous acid, *Nature*, *440*(7081), 195–198, doi:10.1038/nature04603.

Stemmler, K., M. Ndour, Y. Elshorbany, J. Kleffmann, B. D'Anna, C. George, B. Bohn, and M. Ammann (2007), Light induced conversion of nitrogen dioxide into nitrous acid on submicron humic acid aerosol, *Atmos. Chem. Phys.*, *7*(16), 4237–4248.

Stutz, J., B. Alicke, and A. Neftel (2002), Nitrous acid formation in the urban atmosphere: Gradient measurements of NO_2 and HONO over grass in Milan, Italy, *J. Geophys. Res.*, *107*(D22), 8192, doi:10.1029/2001JD000390.

Su, H., Y. F. Cheng, R. Oswald, T. Behrendt, I. Trebs, F. X. Meixner, M. O. Andreae, P. Cheng, Y. Zhang, and U. Poschl (2011), Soil nitrite as a source of atmospheric HONO and OH radicals, *Science*, *333*(6049), 1616–1618, doi:10.1126/science.1207687.

Turanyi, T., A. S. Tomlin, and M. J. Pilling (1993), On the error of the quasi-steady-state approximation, *J. Phys. Chem.*, *97*(1), 163–172, doi:10.1021/j100103a028.

Turner, D. B. (1994), *Estimates of Atmospheric Dispersion in Workbook of Atmospheric Dispersion Estimates: An Introduction to Dispersion Modeling*, pp. 2–1–2–38, Lewis Publishers, Boca Raton, FL.

Winer, A. M., and H. W. Biermann (1994), Long pathlength differential optical-absorption spectroscopy (DOAS) measurements of gaseous HONO, NO_2 and HCHO in the California South Coast Air Basin, *Res. Chem. Intermed.*, *20*(3–5), 423–445, doi:10.1163/156856794X00405.

Wong, K. W., H. J. Oh, B. L. Lefer, B. Rappengluck, and J. Stutz (2011), Vertical profiles of nitrous acid in the nocturnal urban atmosphere of Houston, TX, *Atmos. Chem. Phys.*, *11*(8), 3595–3609, doi:10.5194/acp-11-3595-2011.

Wong, K. W., C. Tsai, B. Lefer, C. Haman, N. Grossberg, W. H. Brune, X. Ren, W. Luke, and J. Stutz (2012), Daytime HONO vertical gradients during SHARP 2009 in Houston, TX, *Atmos. Chem. Phys.*, *12*, 635–652, doi:10.5194/acp-12-635-2012.

Yu, Y., B. Galle, A. Panday, E. Hodson, R. Prinn, and S. Wang (2009), Observations of high rates of NO_2-HONO conversion in the nocturnal atmospheric boundary layer in Kathmandu, Nepal, *Atmos. Chem. Phys.*, *9*(17), 6401–6415.

Zhou, X. L., et al. (2011), Nitric acid photolysis on forest canopy surface as a source for tropospheric nitrous acid, *Nat. Geosci.*, *4*(7), 440–443, doi:10.1038/NGEO1164.

Ziemba, L. D., J. E. Dibb, R. J. Griffin, C. H. Anderson, S. I. Whitlow, B. L. Lefer, B. Rappengluck, and J. Flynn (2010), Heterogeneous conversion of nitric acid to nitrous acid on the surface of primary organic aerosol in an urban atmosphere, *Atmos. Environ.*, *44*(33), 4081–4089, doi:10.1016/j.atmosenv.2008.12.024.